

# Dalitz Plot Analysis of $B^- \rightarrow D^+ \pi^- \pi^-$

T. M. Karbach<sup>1</sup>, representing the *BABAR* Collaboration

<sup>1</sup>*Technische Universität Dortmund*

We present a Dalitz plot analysis of  $B^- \rightarrow D^+ \pi^- \pi^-$  decays, based on a sample of about 383 million  $\Upsilon(4S) \rightarrow B\bar{B}$  decays collected by the *BABAR* detector at the PEP-II asymmetric-energy *B* Factory at SLAC. The analysis has been published previously in [1]. We measure the inclusive branching fraction of the three-body decay to be  $\mathcal{B}(B^- \rightarrow D^+ \pi^- \pi^-) = (1.08 \pm 0.03(\text{stat}) \pm 0.05(\text{syst})) \times 10^{-3}$ . We observe the established  $D_2^{*0}$  and confirm the existence of  $D_0^{*0}$  in their decays to  $D^+ \pi^-$ , where the  $D_2^{*0}$  and  $D_0^{*0}$  are the  $2^+$  and  $0^+$   $c\bar{u}$  P-wave states, respectively. We measure the masses and widths of  $D_2^{*0}$  and  $D_0^{*0}$  to be:  $m_{D_2^*} = (2460.4 \pm 1.2 \pm 1.2 \pm 1.9) \text{ MeV}/c^2$ ,  $\Gamma_{D_2^*} = (41.8 \pm 2.5 \pm 2.1 \pm 2.0) \text{ MeV}$ ,  $m_{D_0^*} = (2297 \pm 8 \pm 5 \pm 19) \text{ MeV}/c^2$ ,  $\Gamma_{D_0^*} = (273 \pm 12 \pm 17 \pm 45) \text{ MeV}$ . The stated errors reflect the statistical and systematic uncertainties, and the uncertainty related to the assumed composition of signal events and the theoretical model.

PACS numbers: 12.15.Hh, 11.30.Er, 13.25.Hw

## I. INTRODUCTION

Orbitally excited states of the *D* meson, denoted as  $D_J$ , provide a unique opportunity to test Heavy Quark Effective Theory (HQET). There are expected to be four P-wave states of positive parity with the quantum numbers  $0^+(j=1/2)$ ,  $1^+(j=1/2)$ ,  $1^+(j=3/2)$  and  $2^+(j=3/2)$ , which are labeled as  $D_0^*$ ,  $D_1$ ,  $D_1'$  and  $D_2^*$ , respectively, where  $j$  is the sum of the spin of the light quark and the angular momentum  $L$ . Conservation of parity and angular momentum restricts the final states and partial waves that are allowed in the decays of the various  $D_J$  mesons. The resonances that decay through a D-wave are expected to be narrow ( $\sim 30 \text{ MeV}/c^2$ ) and the resonances that decay through an S-wave are expected to be wide (a few hundred  $\text{MeV}/c^2$ ). The  $D_2^*$  can only decay via a D-wave and the  $D_0^*$  can only decay via an S-wave. The  $D_1$  and  $D_1'$  may decay via S-wave and D-wave. Fig. 1 shows the spectroscopy of the D-meson excitations and expected transitions. The Belle Collaboration has reported the first observation of the broad  $D_0^*$  and  $D_1'$  mesons in *B* decays [3]. However, the Particle Data Group [4] considers that the  $J$  and  $P$  quantum numbers of the  $D_0^*$  and  $D_1'$  states still need confirmation.

In this analysis, we fully reconstruct the decays of  $B^- \rightarrow D^+ \pi^- \pi^-$  final states [2] and measure the inclusive branching fraction. Then we perform a Dalitz plot analysis to measure the exclusive branching fractions for  $B^- \rightarrow D_0^* \pi^-$  and to study the properties of the  $D_J$  mesons. The decay  $B^- \rightarrow D^+ \pi^- \pi^-$  is expected to be dominated by the intermediate states  $D_2^* \pi^-$  and  $D_0^* \pi^-$  and has a possible contribution from the  $B^- \rightarrow D^+ \pi^- \pi^-$  non-resonant (NR) decay. Also, the  $D^*(2007)^0$  (labeled as  $D_v^*$ ) may contribute as a virtual intermediate state, as well as the  $B^*$  (labeled as  $B_v^*$ ), produced in a virtual process  $B^- \rightarrow B^* \pi^-$ . The data used in this analysis were collected with the *BABAR* detector at the PEP-II asymmetric  $e^+e^-$  storage rings. The *BABAR* detector is described in [1] and in the references therein. The sample consists of  $347.23 \text{ fb}^{-1}$  corresponding to  $382.9 \pm 4.2$  million  $B\bar{B}$  pairs taken on the peak of the  $\Upsilon(4S)$  resonance.

## II. EVENT SELECTION

Five charged particles are selected to reconstruct  $B^- \rightarrow D^+ \pi^- \pi^-$  decays with  $D^+ \rightarrow K^- \pi^+ \pi^+$ . At the  $\Upsilon(4S)$  resonance, *B* mesons can be characterized by two nearly independent kinematic variables, the beam energy substituted mass  $m_{\text{ES}}$  and the energy difference  $\Delta E$ :

$$m_{\text{ES}} = \sqrt{(s/2 + \vec{p}_0 \cdot \vec{p}_B)^2/E_0^2 - p_B^2}, \quad \Delta E = E_B^* - \sqrt{s}/2, \quad (1)$$

where  $E$  and  $p$  are energy and momentum, the subscripts 0 and  $B$  refer to the  $e^+e^-$ -beam system and the  $B$  candidate respectively;  $s$  is the square of the center-of-mass energy and the asterisk labels the CM frame. For  $B^- \rightarrow D^+ \pi^- \pi^-$  signal decays, the  $m_{\text{ES}}$  distribution is well described by a Gaussian resolution function with a width of  $2.6 \text{ MeV}/c^2$  centered at the  $B^-$  mass, while the  $\Delta E$  distribution can be represented by a sum of two Gaussian functions with a common mean near zero and different widths with a combined RMS of  $20 \text{ MeV}$ . The  $\Delta E$  distribution is shown in Fig. 1.

Continuum events are the dominant background. We suppress this background by restricting two topological variables: the magnitude of the cosine of the thrust angle,  $\cos \theta_{th}$ , defined as the angle between the thrust axis of the

selected  $B$  candidate and the thrust axis of the rest of the event; and the ratio of the second to zeroth Fox-Wolfram moment [5],  $R_2$ . Small values of  $R_2$  indicate a more spherical event shape (typical for  $B\bar{B}$  events) while larger values indicate a 2-jet event topology (typical for  $q\bar{q}$  events). We also place restrictions on  $m_{\text{ES}}$  and  $\Delta E$ . Then we fit the  $\Delta E$  distribution to determine the fractions of signal and background events in the selected data sample. The result of the fit is shown in Fig. 1, it yields  $3496 \pm 74$  signal events.

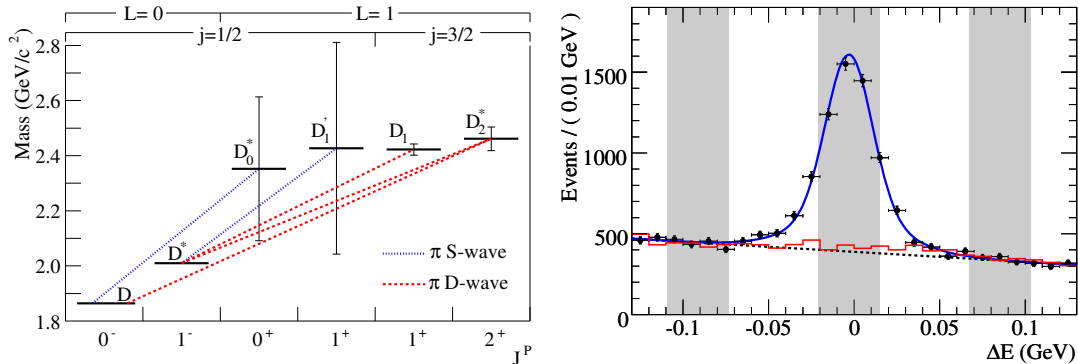


FIG. 1: Left: Mass spectrum [4] of  $c\bar{u}$  states. The vertical bars show the widths. The dotted and dashed lines between the levels show the dominant pion transitions. Although it is not indicated in the figure, the two  $1^+$  states may be mixtures of  $j = 1/2$  and  $j = 3/2$ , and  $D_1^*$  may decay via a D-wave and  $D_1$  may decay via an S-wave. Right:  $\Delta E$  distribution. The points with error bars are data, the red curve is the full fit, the blue dashed curve is the background, the three shaded regions, correspond to the  $\Delta E$  left side- and signal bands. The histogram shown background expected from MC.

To distinguish signal and background in the Dalitz plot studies, we divide the candidates into three subsamples: the  $\Delta E$  signal region, and two  $\Delta E$  sidebands, all defined in Fig. 1. A background MC sample of resonant and continuum events is shown as the histogram in Fig. 1. There is a small amount of peaking, a fit yields  $82 \pm 41$  peaking events. The background subtracted number of signal events is  $N_{\text{sig}} = 3414 \pm 85$ , resulting in the background fraction of  $(30.4 \pm 1.1)\%$ .

### III. DALITZ PLOT ANALYSIS

In this analysis we choose the two  $D\pi$  invariant mass-squared combinations  $x = m^2(D^+\pi_1^-)$  and  $y = m^2(D^+\pi_2^-)$  as the independent variables, where the two like-sign pions are randomly assigned to  $x$  and  $y$ . This has no effect on our analysis since the likelihood function (described below) is explicitly symmetrized with respect to interchange of the two identical particles. We describe the distribution of candidate events in the Dalitz plot in terms of a probability density function (PDF). The PDF is the sum of signal and background components and has the form:

$$\text{PDF}(x, y) = f_{\text{bg}} \frac{B(x, y)}{\int_{\text{DP}} B(x, y) dx dy} + (1 - f_{\text{bg}}) \frac{[S(x, y) \otimes \mathcal{R}] \epsilon(x, y)}{\int_{\text{DP}} [S(x, y) \otimes \mathcal{R}] \epsilon(x, y) dx dy}, \quad (2)$$

where  $S(x, y) \otimes \mathcal{R}$  is the signal term convolved with the signal resolution function,  $B(x, y)$  is the background term,  $f_{\text{bg}}$  is the fraction of background events, and  $\epsilon$  is the reconstruction efficiency. An unbinned maximum likelihood fit to the Dalitz plot is performed in order to maximize the value of  $\mathcal{L} = \prod_{i=1}^{N_{\text{event}}} \text{PDF}(x_i, y_i)$  with respect to the parameters used to describe  $S$ , where  $x_i$  and  $y_i$  are the values of  $x$  and  $y$  for event  $i$ , respectively. It is difficult to find a proper binning at the kinematic boundaries in the  $x$ - $y$ -plane of the Dalitz plot. For this reason, we choose to estimate the goodness-of-fit  $\chi^2$  in the  $\cos\theta$  and  $m_{\text{min}}^2$  plane, which is a rectangular representation of the Dalitz plot. The helicity angle  $\theta$  is the angle between the momentum of the pion from the  $B$  decay and that of the pion of the  $D\pi$  system in the  $D\pi$  restframe;  $m_{\text{min}}^2$  is the lesser of  $x$  and  $y$ . This analysis uses an isobar model formulation in which the signal decays are described by a coherent sum of a number of two-body ( $D\pi$  system + bachelor pion) amplitudes. The orbital angular momentum between the  $D\pi$  system and the bachelor pion is denoted as  $L$ . The total decay matrix element  $\mathcal{M}$  is then given by:

$$\mathcal{M} = \sum_{L=(0,1,2)} \rho_L e^{i\Phi_L} [N_L(x, y) + N_L(y, x)] + \sum_k \rho_k e^{i\Phi_k} [A_k(x, y) + A_k(y, x)], \quad (3)$$

where the first term represents the S-wave ( $L = 0$ ), P-wave ( $L = 1$ ) and D-wave ( $L = 2$ ) non-resonant contributions, the second term stands for the resonant contributions, the parameters  $\rho_k$  and  $\Phi_k$  are the magnitudes and phases of the  $k^{\text{th}}$  resonance, while  $\rho_L$  and  $\Phi_L$  correspond to the magnitudes and phases of the non-resonant contributions with angular momentum  $L$ . The functions  $N_L(x, y)$  and  $A_k(x, y)$  are the amplitudes of non-resonant and resonant terms, respectively. The resonant amplitudes  $A_k(x, y)$  are expressed as  $A_k(x, y) = R_k(m) F_L(p' r') F_L(qr) T_L(p, q, \cos \theta)$ , where  $R_k(m)$  is the  $k^{\text{th}}$  resonance lineshape,  $F_L(p' r')$  and  $F_L(qr)$  are the Blatt-Weisskopf barrier factors [6], and  $T_L(p, q, \cos \theta)$  gives the angular distribution. The parameter  $m(= \sqrt{x})$  is the invariant mass of the  $D\pi$  system. The parameters  $p'$ ,  $p$ ,  $q$  and  $\theta$  are functions of  $x$  and  $y$ . The non-resonant amplitudes  $N_L(x, y)$  are similar to  $A_k(x, y)$  but do not contain resonant mass terms. The Blatt-Weisskopf barrier factors depend on a single parameter,  $r'$  or  $r$ , the radius of the barrier, which we take to be  $1.6 (\text{GeV}/c)^{-1}$ , similarly to Ref. [3]. The functional forms of the  $F_L$  are given in Ref. [1]. For virtual  $D_v^*$  decays,  $D_v^* \rightarrow D^+ \pi^-$ , and virtual  $B_v^*$  production in  $B^- \rightarrow B_v^* \pi^-$ , we use an exponential form factor in place of the Blatt-Weisskopf barrier factor, as discussed in Ref. [3]:  $F(z) = \exp(-(z - z'))$ , where  $z' = r p_v$  for  $D_v^* \rightarrow D^+ \pi^-$  and  $z' = r' p_v$  for  $B^- \rightarrow B_v^* \pi^-$ . Here, we set  $p_v = 0.038 \text{ GeV}/c$ , which gives the best fit. The resonance mass term  $R_k(m)$  describes the intermediate resonance. All resonances in this analysis are parameterized with relativistic Breit-Wigner functions:

$$R_k(m) = \frac{1}{(m_0^2 - m^2) - im_0 \Gamma(m)}, \quad \Gamma(m) = \Gamma_0 \left( \frac{q}{q_0} \right)^{2L+1} \left( \frac{m_0}{m} \right) F_L^2(qr), \quad (4)$$

where  $m_0$  and  $\Gamma_0$  are the values of the resonance pole mass and decay width, respectively. The terms  $T_L(p, q, \cos \theta)$  describe the angular distribution of final state particles and are based on the Zemach tensor formalism [7]. The definitions are given in [1]. The signal function is then given by  $S(x, y) = |\mathcal{M}|^2$ .

In this analysis, the masses of  $D_v^*$  and  $B_v^*$  are taken from the world averages [4] while their widths are fixed at 0.1 MeV; the magnitude  $\rho_k$  and phase  $\Phi_k$  of the  $D_2^*$  amplitude are fixed to 1 and 0, respectively, while the masses and widths of the  $D_J$  resonances and the other magnitudes and phases are free parameters to be determined in the fit. The effect of varying the masses of  $D_v^*$  and  $B_v^*$  between 0.001 and 0.3 MeV is negligible compared to the other model-dependent systematic uncertainties.

The fit fraction for the  $k^{\text{th}}$  decay mode is defined as the integral of the resonance decay amplitudes divided by the coherent matrix element squared for the complete Dalitz plot:

$$f_k = \frac{\int_{\text{DP}} |\rho_k (A_k(x, y) + A_k(y, x))|^2 dx dy}{\int_{\text{DP}} |\mathcal{M}|^2 dx dy}. \quad (5)$$

The detector has a finite resolution. For the narrow resonance  $D_2^*$  with the expected width of about 40 MeV, the signal resolution needs to be taken into account. We study the resolution on MC simulated events. We find the resolution to be independent of  $\cos \theta$  for truth-matched events, and we describe it by a sum of two Gaussian functions with a common mean. The signal resolution for an invariant mass of the  $D\pi$  combination around the  $D_2^*$  region is about  $3 \text{ MeV}/c^2$ . There is a small self crossfeed (SCF) component, which varies from 0.5% to 4.0% with  $\cos \theta$ . For this component, also the resolution varies with  $\cos \theta$ , which we take into account. We also check the estimated biases in the fitted parameters due to uncertainties in the signal resolution functions are small.

The signal term is modified in order to take into account the particle detection efficiency. Since different regions of the Dalitz plot correspond to different event topologies, the efficiency is not expected to be uniform over the Dalitz plot. We determine the efficiency function,  $\epsilon(x, y)$ , by fitting twice a large sample of  $B^- \rightarrow D^+ \pi^- \pi^-$  MC: before and after the final selection was applied. The properly normalized ratio of the fit functions gives  $\epsilon(x, y)$ . The efficiency is flat in the center of the Dalitz plot, and drops close to its boundaries.

The background distribution is modeled using an analytic function describing MC background events. Since we find the Dalitz plot distributions of  $\Delta E$  sideband events in data and in MC to be consistent within their statistics, we are confident that the MC simulation can accurately represent the background in the signal region.

#### IV. PHYSICS RESULTS

The total  $B^- \rightarrow D^+ \pi^- \pi^-$  branching fraction is calculated using the relation:  $\mathcal{B} = N_{\text{signal}} / (\bar{\epsilon} \cdot \mathcal{B}(D^+) \cdot 2N(B^+ B^-))$ , where  $N_{\text{signal}} = 3414 \pm 85$ ,  $\bar{\epsilon}$  is the average efficiency,  $\mathcal{B}(D^+) \equiv \mathcal{B}(D^+ \rightarrow K^- \pi^+ \pi^+) = (9.22 \pm 0.21) \%$ , and the total number of  $B^+ B^-$  events  $N(B^+ B^-) = (197.2 \pm 3.1) \times 10^6$ . The measured total branching fraction is  $\mathcal{B}(B^- \rightarrow D^+ \pi^- \pi^-) = (1.08 \pm 0.03(\text{stat})) \times 10^{-3}$ .

The Dalitz plot distribution for data is included in [1]. Since the composition of events in the Dalitz plot and their distributions are not known a priori, we have tried a variety of different assumptions. In particular, we test the

inclusion of various components, such as the virtual  $D_v^*$  and  $B_v^*$  as well as S-, P-, and D-wave modeling of the non-resonant component, in addition to the expected components of  $D_2^*$ ,  $D_0^*$ , and background. We choose as the nominal fit model the one with the  $D_2^*$ ,  $D_0^*$ ,  $D_v^*$ ,  $B_v^*$ , and P-wave non-resonant components considered. It produces the best fit quality with the smallest number of components. The P-wave non-resonant component is an addition to the fit model used in the previous measurement from Belle [3]. The detailed fit results are:  $m_{D_2^*} = 2460.4 \pm 1.2$ ,  $\Gamma_{D_2^*} = 41.8 \pm 2.5$ ,  $m_{D_0^*} = 2297 \pm 8$ ,  $\Gamma_{D_0^*} = 273 \pm 12$ ,  $f_{D_2^*} = 32.2 \pm 1.3$ ,  $\Phi_{D_2^*} = 0.0$  fixed,  $f_{D_0^*} = 62.8 \pm 2.5$ ,  $\Phi_{D_0^*} = -2.07 \pm 0.06$ ,  $f_{D_v^*} = 10.1 \pm 1.4$ ,  $\Phi_{D_v^*} = 3.00 \pm 0.12$ ,  $f_{B_v^*} = 4.6 \pm 2.6$ ,  $\Phi_{B_v^*} = 2.89 \pm 0.21$ ,  $f_{\text{P-NR}} = 5.4 \pm 2.4$ ,  $\Phi_{\text{P-NR}} = -0.89 \pm 0.18$ ,  $f_{\text{bg}} = 30.4$  fixed, where masses are in units of  $\text{MeV}/c^2$ , widths in MeV, fractions in %, and angles in radians. All errors are statistical only. The total  $\chi^2$  over degrees of freedom is 220/153. The details of the other fit models in question are detailed in Ref. [1]. Ref. [8] argues for an addition of a  $D\pi$  S-wave state near the  $D\pi$  system threshold to the model of the  $D\pi\pi$  final state. We have performed according tests [1], which all yielded worse fit qualities than the nominal fit.

The nominal fit model results in the following branching fractions:  $\mathcal{B}(B^- \rightarrow D_2^* \pi^-) \times \mathcal{B}(D_2^* \rightarrow D^+ \pi^-) = (3.5 \pm 0.2) \times 10^{-4}$  and  $\mathcal{B}(B^- \rightarrow D_0^* \pi^-) \times \mathcal{B}(D_0^* \rightarrow D^+ \pi^-) = (6.8 \pm 0.3) \times 10^{-4}$ , where the errors are statistical only. Fig. 2a-c show the  $m_{\text{min}}^2(D\pi)$ ,  $m_{\text{max}}^2(D\pi)$ , and  $m^2(\pi\pi)$  projections, respectively, while Fig. 3a and 3b show the  $\cos\theta$  distributions for the  $D_0^*$  and  $D_2^*$  mass regions, respectively. The distributions show good agreement between the data and the fit. The angular distribution in the  $D_2^*$  mass region is clearly visible and is consistent with the expected D-wave distribution of  $|\cos^2\theta - 1/3|^2$  for a spin-2 state. In addition, the  $D_0^*$  signal and the reflection of  $D_2^*$  can be easily distinguished in the  $m_{\text{min}}^2(D\pi)$  and  $m_{\text{max}}^2(D\pi)$  projection, respectively. The lower edge of  $m_{\text{min}}^2(D\pi)$  is better described with the  $D_v^*$  component included than without.

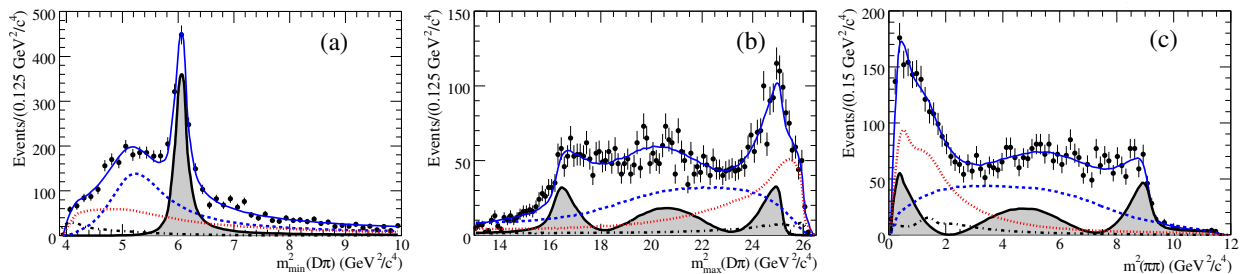


FIG. 2: Result of the nominal fit to the data: projections on (a)  $m_{\text{min}}^2(D\pi)$ , (b)  $m_{\text{max}}^2(D\pi)$ , and (c)  $m^2(\pi\pi)$ . The points are the data, the solid curves represent the nominal fit. The shaded areas show the  $D_2^*$  contribution, the dashed curves show the  $D_0^*$  signal, the dash-dotted curves show the  $D_v^*$  and  $B_v^*$  signals, and the dotted curves show the background.

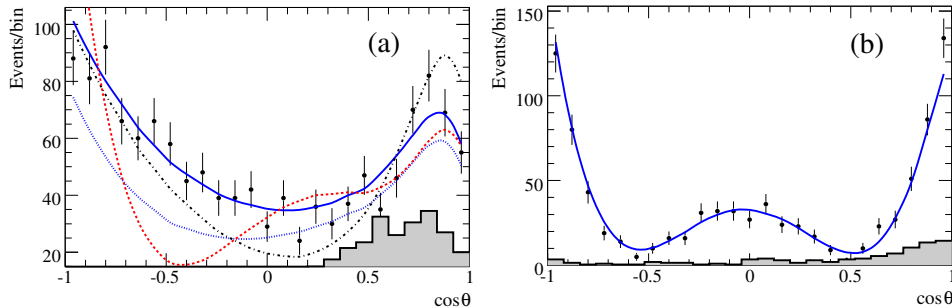


FIG. 3: Result of the nominal fit to the data: the  $\cos\theta$  distributions for (a)  $4.5 < m^2(D\pi) < 5.5 \text{ GeV}^2/c^4$  region and (b)  $5.9 < m^2(D\pi) < 6.2 \text{ GeV}^2/c^4$  region. The points with error bars are data, the solid curves represent the nominal fit. The dashed, dash-dotted and dotted curves in (a) show the fit of hypotheses 2-4 in Table I, respectively. The shaded histograms show the  $\cos\theta$  distributions from  $\Delta E$  sidebands in data.

Table I shows the NLL and  $\chi^2/\text{NDF}$  values for the nominal fit and for the fits with the broad resonance  $D_0^*$  excluded or with the  $J^P$  of the broad resonance replaced by other quantum numbers. In all cases, the NLL and  $\chi^2/\text{NDF}$  values are significantly worse than that of the nominal fit. Fig. 3a illustrates the helicity distributions in the  $D_0^*$  mass region from hypothesis 2-4; clearly the nominal fit gives the best description of the data. We conclude that a broad spin-0 state  $D_0^*$  is required in the fit to the data. The same conclusion is obtained when performing the same tests using the alternative non-nominal fit models.

Hypothesis	Model	NLL	$\chi^2/\text{NDF}$
	nominal fit	22970	220/153
1	$D_2^*$ , $D_v^*$ , $B_v^*$ , P-NR	23761	1171/143
2	$D_2^*$ , $D_v^*$ , $B_v^*$ , P-NR, ( $2^+$ )	23699	991/144
3	$D_2^*$ , $D_v^*$ , $B_v^*$ , P-NR, ( $1^-$ )	23427	638/135
4	$D_2^*$ , $D_v^*$ , $B_v^*$ , P-NR, S-NR	23339	652/157

TABLE I: Comparison of the models with different resonance composition. The labels, S-NR and P-NR, denote the S- and P-wave non-resonant contributions.

The systematic uncertainties under consideration are detailed in Ref. [1]. The systematic effects considered include the number of  $B^+B^-$  events, tracking efficiencies, particle identification, uncertainty on the background shapes, external  $D^+$  branching fraction, and fit bias.

## V. SUMMARY

In conclusion, we measure the total branching fraction of the  $B^- \rightarrow D^+\pi^-\pi^-$  decay to be  $\mathcal{B}(B^- \rightarrow D^+\pi^-\pi^-) = (1.08 \pm 0.03(\text{stat}) \pm 0.05(\text{syst})) \times 10^{-3}$ . Analysis of the  $B^- \rightarrow D^+\pi^-\pi^-$  Dalitz plot using the isobar model confirms the existence of a narrow  $D_2^*$  and a broad  $D_0^*$  resonance as predicted by HQET. The mass and width of  $D_2^*$  are determined to be  $m_{D_2^*} = (2460.4 \pm 1.2(\text{stat}) \pm 1.2(\text{syst}) \pm 1.9(\text{mod})) \text{ MeV}/c^2$ ,  $\Gamma_{D_2^*} = (41.8 \pm 2.5(\text{stat}) \pm 2.1(\text{syst}) \pm 2.0(\text{mod})) \text{ MeV}$ , while of the  $D_0^*$  they are:  $m_{D_0^*} = (2297 \pm 8(\text{stat}) \pm 5(\text{syst}) \pm 19(\text{mod})) \text{ MeV}/c^2$ ,  $\Gamma_{D_0^*} = (273 \pm 12(\text{stat}) \pm 17(\text{syst}) \pm 45(\text{mod})) \text{ MeV}$ , where the third uncertainty is related to the assumed composition of signal events and the Blatt-Weisskopf barrier factors. The measured masses and widths of both states are consistent with the world averages [4] and the predictions of some theoretical models (see references in [1]). We have also obtained exclusive branching fractions for  $D_2^*$  and  $D_0^*$  production:  $\mathcal{B}(B^- \rightarrow D_2^*\pi^-) \times \mathcal{B}(D_2^* \rightarrow D^+\pi^-) = (3.5 \pm 0.2(\text{stat}) \pm 0.2(\text{syst}) \pm 0.4(\text{mod})) \times 10^{-4}$ ,  $\mathcal{B}(B^- \rightarrow D_0^*\pi^-) \times \mathcal{B}(D_0^* \rightarrow D^+\pi^-) = (6.8 \pm 0.3(\text{stat}) \pm 0.4(\text{syst}) \pm 2.0(\text{mod})) \times 10^{-4}$ . Our results of the masses, widths and branching fractions are consistent with but more precise than previous measurements performed by Belle [3]. The relative phase of the scalar and tensor amplitude is measured to be  $\Phi_{D_0^*} = -2.07 \pm 0.06(\text{stat}) \pm 0.09(\text{syst}) \pm 0.18(\text{mod}) \text{ rad}$ .

## VI. ACKNOWLEDGEMENTS

The author is thankful to the *BABAR* Collaboration, its funding agencies, and the organizers of the HADRON09 conference.

- 
- [1] BABAR Collaboration, B. Aubert *et al.*, Phys. Rev. D **79**, 112004 (2009).
  - [2] Charged conjugate states are implied throughout the paper.
  - [3] Belle Collaboration, K. Abe *et al.*, Phys. Rev. D **69**, 112002 (2004).
  - [4] Particle Data Group, Particle Data Group, C. Amsler *et al.*, Phys. Lett. B **667**, 1 (2008).
  - [5] G. C. Fox and S. Wolfram, Phys. Rev. Lett. **41**, 1581 (1978).
  - [6] J. Blatt and V. Weisskopf, Theoretical Nuclear Physics, p.361, New York: John Wiley and Sons (1952).
  - [7] C. Zemach, Phys. Rev. B140, 97,109 (1965).
  - [8] D. V. Bugg, J. Phys. G **36**, 075003 (2009).